

# Organic & Biomolecular Chemistry

Accepted Manuscript



This is an *Accepted Manuscript*, which has been through the Royal Society of Chemistry peer review process and has been accepted for publication.

*Accepted Manuscripts* are published online shortly after acceptance, before technical editing, formatting and proof reading. Using this free service, authors can make their results available to the community, in citable form, before we publish the edited article. We will replace this *Accepted Manuscript* with the edited and formatted *Advance Article* as soon as it is available.

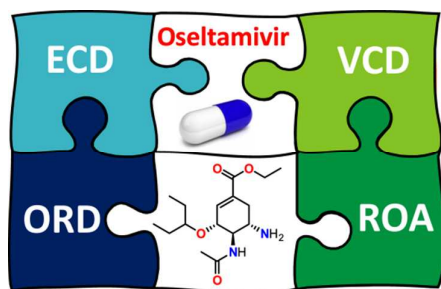
You can find more information about *Accepted Manuscripts* in the [Information for Authors](#).

Please note that technical editing may introduce minor changes to the text and/or graphics, which may alter content. The journal's standard [Terms & Conditions](#) and the [Ethical guidelines](#) still apply. In no event shall the Royal Society of Chemistry be held responsible for any errors or omissions in this *Accepted Manuscript* or any consequences arising from the use of any information it contains.

# Configurational and Conformational Study of (–)-Oseltamivir Using a Multi-Chiroptical Approach

Marcin Górecki\*

Institute of Organic Chemistry of the Polish Academy of Sciences, Kasprzaka St. 44/52,  
01-224 Warsaw, Poland, E-mail: marcin.gorecki@icho.edu.pl



## ABSTRACT

To better understand structure-activity relationship (SAR) results, closely related to the structural features of (–)-Oseltamivir, four chiroptical methods, *i.e.* electronic circular dichroism (ECD), optical rotatory dispersion (ORD), vibrational circular dichroism (VCD), and Raman optical activity (ROA), utilizing different solvents, were employed in an effort to discover a set of the most probable conformations. Such multi-chiroptical approach supported by the quantum chemical calculations pointed out that different conformers are stable in chloroform, acetonitrile and water solutions of (–)-Oseltamivir. This way, the most probable structures responsible for reported SAR results were established for the first time. It turned out that one of the predominant conformers in a solution is in excellent agreement with the X-ray analysis derived solid-state structure determined for (–)-Oseltamivir Phosphate.

## INTRODUCTION

Chirality plays a key role in any interaction of living matter with the environment. One of the most immediate and essential consequences of chirality is seen in pharmaceutical sciences. Most receptors in human body are chiral and as a result, may interact in a different manner with the enantiomers of a chiral drug, causing distinct biological and pharmacological effects for each of them. Consequently, the pharmaceutical regulatory authorities recognized the essential role played by stereochemistry. Applicants are now prompted to identify the absolute stereostructure of new drugs, and to separate and determine the bioactivity of all possible stereoisomers.<sup>1-3</sup> The influence of stereochemistry on the behaviour of bioactive

compounds cannot be overestimated. It has a significant impact on a number of molecular properties such as chemical reactivity, catalytic, and biological activities. Clearly, the chiral analysis is crucial in this combination and provides the key contribution to the better understanding of biorecognition processes including the binding of drugs to their targets and the modulation of their function. Such information is essential for the rational design of new potent and selective drugs, as well as the subsequent optimization of their pharmacokinetic profiles.<sup>2,3</sup> Since many active pharmaceutical ingredients (APIs) possess chiral motifs, a determination of the absolute structure (configuration and conformation) continues to be an important challenge in the organic and medicinal chemistry.

The significantly expanded assortment of commercially available instruments, relying on electronic (ECD, ORD) and vibrational (VCD, ROA) transitions, for measuring different chiroptical phenomena opens new pathways to study conformation and interactions with the environment of chiral molecules in the solution phase.<sup>4-12</sup> Polavarapu pointed out<sup>13,14</sup> that simultaneous use of different chiroptical techniques increases the confidence level of the stereochemical analysis of chiroptical data. Nevertheless, chiroptical techniques can be sensitive to environmental perturbations and their level of sensitivity may vary.

According to the report of Global Industry Analysts, Inc., approximately 95% of pharmaceutical drugs will be chiral by the year 2020. Since it is not often possible to get suitable crystals for the X-ray analysis, there is a strong necessity to develop methods for direct and fast analysis of chiral compounds in solution. In addition to the absolute configuration(s), the knowledge about the relevant conformers in solution plays a critical role in SAR and molecular docking studies. One of the best choices, to carry out such research, is the complementary approach utilizing experimental chiroptical methods in combination with corresponding quantum chemical calculations. It is nowadays more than reasonable and legitimate for APIs to undertake such a comprehensive conformational analysis based on the theoretical computations and experiment.

Interestingly, there are no literature reports indicating that such a study ever took place for (–)-Oseltamivir, also known as the Tamiflu®, which is presently one of the most active drugs for the treatment of influenza A and B viruses, including avian flu (Fig. 1).

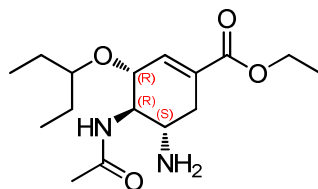


**Fig. 1.** Structure of (3*R*,4*R*,5*S*)-(-)-Oseltamivir. Chemical name: (3*R*,4*R*,5*S*)-4-acetylamino-5-amino-3-(1-ethylpropoxy)-1-cyclohexene-1-carboxylic acid ethyl ester.

(-)-Oseltamivir is a second-generation oral neuraminidase inhibitor, and it is currently considered the only effective drug for avian flu.<sup>15</sup> As a consequence, many organic chemists have studied its effective synthesis and published a large number of synthetic methods.<sup>16,17</sup> In 2013 for the first time, after an incredible effort, the solid-phase crystallographic structure of (-)-Oseltamivir Phosphate was obtained by means of a single crystal X-ray diffraction with synchrotron radiation.<sup>18,19</sup> However, the conformation of (-)-Oseltamivir in solution phase was not addressed. In order to fill this gap, the present study reports the chiroptical spectroscopic investigations. The emphasis is focused on particular information that can be extracted from the results obtained using multiple methods, concerning conformational equilibrium in chloroform, acetonitrile, and water solution.

## RESULTS AND DISCUSSION

A fundamental prerequisite for the successful computational calculations of any chiroptical response is the knowledge of all relevant conformational species of the investigated molecule, since all conformers present in the thermodynamic equilibrium contribute to the *net* spectrum.<sup>20</sup> Therefore, the results of a thorough conformational analysis are presented first, followed by the verification of these conclusions by combined results from four available chiroptical methods, along with extensive theoretical simulations of their spectra in solution. Finally, a comparison of molecular arrangement of atoms for one of the lowest energy conformation in solution with that found in a solid phase (based on the X-ray data) is made.

### Conformational Analysis

Due to the high flexibility of the side chains in (-)-Oseltamivir, resulting from the large number of rotatable bonds, a determination of the most relevant group of conformers is not a trivial task. To resolve this problem, the following search strategy was used. In the first step, the conformational search at the molecular mechanics level was carried out within 10 kcal/mol energy window using CONFLEX 7<sup>21-23</sup> software with MMFF94s force field (static variant of MMFF94). As a result, a total of 1150 conformations were identified. Next these geometries were optimized in the framework of the density functional theory (DFT) using Gaussian09<sup>24</sup> at the B3LYP/6-31(d) level in order to reduce their number as well as to remove

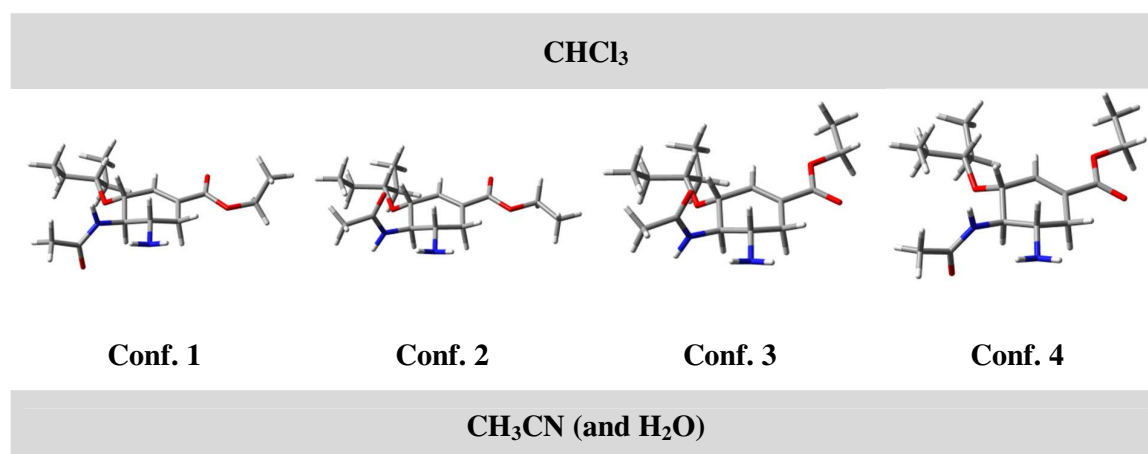
conformers not fitting the narrower 5 kcal/mol energy range, which, by definition, would not make a significant contribution to the overall population. Then, the remaining 24 conformers were re-optimized using higher levels of approximation. The exact knowledge of a population of different conformers is critical for the accurate computational prediction of chiroptical properties.<sup>25</sup> Therefore, in order to exclude the possibility that the population of identified conformers depends on the level of theory used in computation, all 24 structures were optimized under the following levels of theory: B3LYP/TZVP, B3LYP/6-311++G(2d,2p), B3LYP/aug-cc-pVDZ, and CAM-B3LYP/aug-cc-pVDZ, in combination with the implicit polarizable continuum model (PCM)<sup>26</sup>, to reflect solvent effects using the dielectric constant of chloroform ( $\epsilon = 4.71$ ), acetonitrile ( $\epsilon = 35.69$ ), and water ( $\epsilon = 78.36$ ). The solvents were chosen according to the expected conditions during the experimental measurements of chiroptical data and the requirement for transparency in UV and IR regions. On the other hand, different dielectric constants of a solvent provide an approximate degree of the solvent's polarity,<sup>27</sup> therefore the solvent-dependency of the title molecule is provided. What is more, it is well known that solvent has an effect on the population of conformers because of different physical intermolecular solute-solvent interaction forces (*e.g.* ion-dipole, dipole-dipole, dipole-induced dipole, aggregation, hydrogen bonding, etc.).<sup>27-29</sup> Consequently, the presence of such groups as amino and acetyl amino in (-)-Oseltamivir molecule opens up possibilities for creating hydrogen bonds in solution of acetonitrile or water. The implicit solvent model (PCM) is not efficient in evaluating intramolecular interactions, however such a study is beyond the scope of the current work.

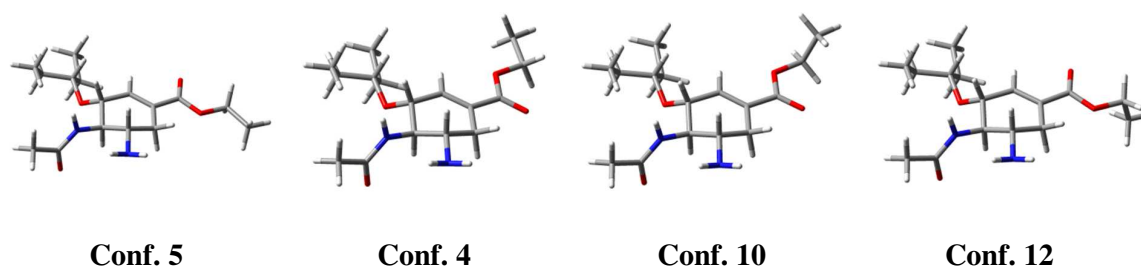
The relative thermal free energy values ( $\Delta G$ ) of stable conformers found in the range of 5 kcal/mol led to similar results, irrespectively of the level of theory used. Therefore, only the geometries obtained from B3LYP/aug-cc-pVDZ/PCM(CHCl<sub>3</sub>) and B3LYP/aug-cc-pVDZ/PCM(CH<sub>3</sub>CN) level were taken into account and used for predicting ECD, ORD, and VCD spectra. Since ROA experiments were conducted exclusively in water solution, the geometries of the relevant conformers from the B3LYP/aug-cc-pVDZ/PCM(H<sub>2</sub>O) theory level were also included. The summary of the conformational search for the (-)-Oseltamivir with relative Gibbs free energies ( $\Delta G$ ) and populations are shown in Table 1. For clarity, conformers with estimated population of less than 1% in equilibrium were excluded. Thus, according to Boltzmann distribution, among 24 possible conformers, 20 are significant in chloroform and they cover *ca.* 97% of all the found structures (Table 1), while there are 13 such conformers in acetonitrile and water. The remaining conformers (*ca.* 3%) are shown in

Table S1 in the Supporting Information. Four of the most abundant conformers are depicted in Fig. 2, while others are shown in Fig. S1 in the Supporting Information.

**Table 1.** An overview of the conformational search for (–)-Oseltamivir. Conformer populations were calculated using the Gibbs free energy  $\Delta G$  (kcal/mol) at the B3LYP/aug-cc-pVDZ level of theory using PCM model for chloroform, acetonitrile and water. Boltzmann weights are based on the  $\Delta G$  at 298 K. The accuracy of molar fractions of particular conformers is far less than the number of decimal places given in the table. This accuracy, however, is kept to show the relative trend of the conformational composition.

B3LYP/aug-cc-pVDZ								
in CHCl <sub>3</sub> ( $\epsilon = 4.71$ )			in CH <sub>3</sub> CN ( $\epsilon = 35.69$ )			in H <sub>2</sub> O ( $\epsilon = 78.36$ )		
	$\Delta G$	$P(\%)$		$\Delta G$	$P(\%)$		$\Delta G$	$P(\%)$
<b>Conf. 1</b>	0.00	9.98	<b>Conf. 5</b>	0.00	16.98	<b>Conf. 5</b>	0.00	16.65
<b>Conf. 2</b>	0.01	9.74	<b>Conf. 4</b>	0.14	13.45	<b>Conf. 4</b>	0.10	14.12
<b>Conf. 3</b>	0.08	8.67	<b>Conf. 10</b>	0.27	10.72	<b>Conf. 10</b>	0.24	11.01
<b>Conf. 4</b>	0.22	6.90	<b>Conf. 12</b>	0.30	10.21	<b>Conf. 12</b>	0.28	10.46
<b>Conf. 5</b>	0.24	6.66	<b>Conf. 9</b>	0.37	9.15	<b>Conf. 9</b>	0.29	10.25
<b>Conf. 6</b>	0.28	6.22	<b>Conf. 1</b>	0.41	8.46	<b>Conf. 1</b>	0.49	7.34
<b>Conf. 7</b>	0.28	6.18	<b>Conf. 14</b>	0.47	7.64	<b>Conf. 14</b>	0.49	7.27
<b>Conf. 8</b>	0.30	6.05	<b>Conf. 8</b>	0.54	6.86	<b>Conf. 8</b>	0.61	5.94
<b>Conf. 9</b>	0.33	5.68	<b>Conf. 17</b>	0.83	4.17	<b>Conf. 17</b>	0.82	4.14
<b>Conf. 10</b>	0.48	4.42	<b>Conf. 13</b>	0.89	3.76	<b>Conf. 13</b>	0.85	3.95
<b>Conf. 11</b>	0.48	4.41	<b>Conf. 7</b>	1.37	1.68	<b>Conf. 20</b>	1.10	2.60
<b>Conf. 12</b>	0.54	4.01	<b>Conf. 2</b>	1.54	1.25	<b>Conf. 22</b>	1.59	1.13
<b>Conf. 13</b>	0.69	3.12	<b>Conf. 3</b>	1.56	1.21	<b>Conf. 7</b>	1.65	1.02
<b>Conf. 14</b>	0.74	2.84						
<b>Conf. 15</b>	0.75	2.83						
<b>Conf. 16</b>	0.80	2.57						
<b>Conf. 17</b>	0.81	2.55						
<b>Conf. 18</b>	1.12	1.50						
<b>Conf. 19</b>	1.12	1.51						
<b>Conf. 20</b>	1.13	1.47						



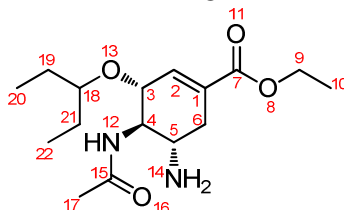


**Fig. 2.** Most abundant conformers of (-)-Oseltamivir calculated at the B3LYP/aug-cc-pVDZ level using PCM model for chloroform, and acetonitrile or water.

According to the calculations of conformational species performed in three representative solvents, *i.e.* chloroform, acetonitrile, and water, there are apparent differences between chloroform and acetonitrile/water. In polar aprotic and protic solvents (acetonitrile and water) there is almost the same composition of conformers. Small differences are occurring only between conformers with distribution lower than 3%, but should not have any noticeable influence on the averaged spectra. To simplify the discussion, one may assume that the same group of conformers is present in both of these solvents. In contrast, the PCM model indicates the presence of a different group of conformers in chloroform, indicating *ipso facto* the influence of solvent on conformer populations. The quantitative comparison between the found conformers is summarized in Table 2. One can notice that the most abundant conformers (**Conf. 1** and **Conf. 5**) have identical orientation of acetylamino and pentyl ether groups in both solvents, and that they differ only in orientation of ethyl group in ester moiety. Despite this, not surprisingly, all structures have the same half-chair conformation of cyclohexene ring, since it is the most stable conformation (Fig. S1) which cyclohexene ring can adopt.<sup>30</sup> For this reason, the various conformers of (-)-Oseltamivir are determined by the flexible substituents located at *equatorial* C4 (acetylamino group), *equatorial* C3 (pentyl ether group), and C1 (ester group) positions. All conformers have a positive torsion angle (*ca.* +53°) between *equatorial* amine (C5) and amide (C4) groups, thereby indicating a presence of the *gauche* conformer in which the steric interactions between these groups are minimized.

Comprehensive analysis of the identified conformers led to the conclusion that they can be divided into two families, depending on the sign of diagnostic torsion angle that includes amide substituent *i.e.* C5-C4-N12-C15. The numbering of atoms is given in the top of Table 2. In the first family this torsion angle is negative, while in the second it is positive. The results, divided into apolar and polar solvents are collected in Table 2. For better understanding of the complex conformational equilibrium in solution, the graphical bars visualization is present for all conformers found in the range of 5 kcal/mol.

**Table 2.** Overview of the conformational search for the (–)-Oseltamivir with four representative torsion angles [°]. Conformer populations were calculated using the Gibbs free energy  $\Delta G$  (kcal/mol) at the B3LYP/aug-cc-pVDZ using PCM for chloroform and acetonitrile. The results from application of PCM model for water solution are not listed, since they are almost consistent with acetonitrile (see Table 1). The length of bars is corresponding to computed values of torsional angles.



CHCl <sub>3</sub>					CH <sub>3</sub> CN						
Conf.	$\Delta G$ [kcal/mol]	C5-C4-N12-C15	C2-C1-C7-O11	C7-O8-C9-C10	O13-C18-C19-C20	Conf.	$\Delta G$ [kcal/mol]	C5-C4-N12-C15	C2-C1-C7-O11	C7-O8-C9-C10	O13-C18-C19-C20
Conf. 1	0.00	-120	4	88	-179	Conf. 5	0.00	-121	3	179	-179
Conf. 2	0.01	81	2	-180	-180	Conf. 4	0.14	-120	-179	-88	-179
Conf. 3	0.08	82	-179	-179	-179	Conf. 10	0.27	-120	-179	-88	-179
Conf. 4	0.22	-121	-179	-179	-179	Conf. 12	0.30	-120	-179	-179	-88
Conf. 5	0.24	-122	4	179	-179	Conf. 9	0.37	-120	-179	87	-179
Conf. 6	0.28	82	-179	-87	-179	Conf. 1	0.41	-120	4	88	-179
Conf. 7	0.28	82	88	-179	-179	Conf. 14	0.47	-120	5	-88	-179
Conf. 8	0.30	-122	5	179	-88	Conf. 8	0.54	-121	4	179	-88
Conf. 9	0.33	-121	87	-179	-179	Conf. 17	0.83	-120	-179	-87	-88
Conf. 10	0.48	-120	-179	-88	-179	Conf. 13	0.89	-121	-179	87	-84
Conf. 11	0.48	80	-180	-84	-84	Conf. 7	1.37	82	-179	87	-179
Conf. 12	0.54	-122	-179	-179	-88	Conf. 2	1.54	81	3	-180	-179
Conf. 13	0.59	-123	88	-88	-179	Conf. 3	1.56	82	-179	-180	-179
Conf. 14	0.74	-121	5	-88	-179	Conf. 22	1.57	-121	8	-88	-88
Conf. 15	0.75	80	-87	-88	-88	Conf. 6	1.81	82	-179	-88	-180
Conf. 16	0.80	89	-180	-88	-88	Conf. 11	1.88	89	-179	-180	-84
Conf. 17	0.81	-120	-180	-87	-84	Conf. 15	2.10	89	4	-180	-84
Conf. 18	1.12	81	3	88	-179	Conf. 16	2.23	80	-179	-88	-84
Conf. 19	1.12	82	2	-88	-179	Conf. 19	2.44	82	3	-88	-179
Conf. 20	1.13	-122	5	88	-84	Conf. 24	2.60	80	4	88	-84
Conf. 21	1.46	80	4	-88	-84	Conf. 18	2.62	82	4	88	-179
Conf. 22	1.63	-122	6	-87	-84	Conf. 23	2.99	89	-179	87	-84
Conf. 23	1.65	89	-179	88	-84	Conf. 21	3.10	89	4	-88	-88
Conf. 24	1.69	80	3	87	-84	Conf. 20	14.50	-124	4	87	-84

The key structural difference among the conformers found in chloroform and acetonitrile/water solutions relates to the rotation of amide substituent at C4 position. Thus, in chloroform there are 54% of species with negative C5-C4-N12-C15 torsion angle (*ca.* -120 °), while in acetonitrile there are 93% of such species. The percentage amount of conformers, separated by the almost planar torsion angle C2-C1-C7-O11, does not depend on the solvent type, so equal population amounting to 56% exists both in chloroform and acetonitrile. It is also worth noting that among the found conformers, besides their categorization in appropriate families, the torsion angle C7-O8-C9-C10, which includes ester group, has the value of either *ca.* ±180 ° or *ca.* ±80 °, however the torsion angle which characterises the orientation of substituent at C3, *i.e.* O13-C18-C19-C20, amounts to either *ca.* -170 ° or *ca.* -64 °.

Seeing that the obtained conformers adopted conformation with the least steric hindrance, the results of conformational search seem to be reasonable. Moreover, the slight difference in the number of conformers in chloroform and acetonitrile/water (20 *vs.* 16 within

2 kcal/mol, respectively) indicates little effect of solvent on conformers' geometries in equilibrium. However, the smaller number of conformers in acetonitrile/water can be attributed to the reduced conformational mobility in these solvents due to the hydrogen bonding.

### Analysis of ECD spectra

The UV and ECD spectra were recorded in hexane, chloroform, acetonitrile and water solutions, respectively (Table 3, Fig. 3). Due to the UV cut-off point of chloroform at *ca.* 230 nm, and, as a result, a lack of ability to register spectrum in range below the cut-off, hexane was chosen as another apolar solvent, and two additional ECD bands were recorded in its spectrum.

**Table 3.** UV and ECD data of (–)-Oseltamivir recorded in hexane, acetonitrile, and water. UV and ECD values are given as  $\epsilon$  ( $\lambda_{\max}/\text{nm}$ ) and  $\Delta\epsilon$  ( $\lambda_{\max}/\text{nm}$ ), respectively.

Solvent	UV, $\epsilon / \text{dm}^3 \text{mol}^{-1} \text{cm}^{-1}$		ECD, $\Delta\epsilon / \text{dm}^3 \text{mol}^{-1} \text{cm}^{-1}$		
	$\lambda_{\max}$ (nm)	$\epsilon$	$\lambda_{\max}$ (nm)	$\Delta\epsilon$	$\lambda_{\max}$ (nm)
Hex	192.6	11200	196.6	+2.6	255.4
CHCl <sub>3</sub>	*	*	*	*	255.0
CH <sub>3</sub> CN	193.4	13700	191.8	+4.9	256.2
H <sub>2</sub> O	192.2	13500	191.2	+5.8	252.6

# shoulder, \* not recorded due to the cut-off point

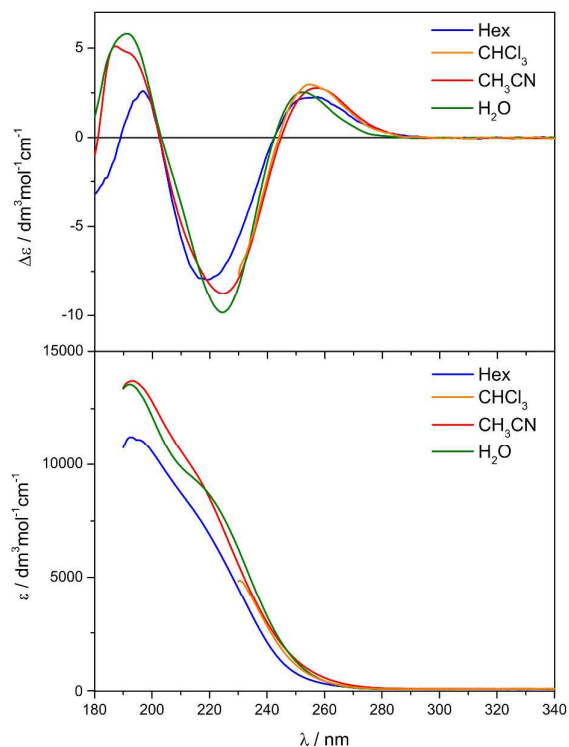


**Fig. 3.** Experimental ECD (top) and UV (bottom) spectra of (–)-Oseltamivir recorded in hexane, chloroform, acetonitrile, and water. Note that the experimental spectrum in chloroform due to cut-off point can be recorded to *ca.* 230 nm.

The ECD curves measured in solvents with different polarity show no significant differences in positions of Cotton effects (CEs) and their intensity (Table 3, Fig. 3). The experimental data exhibits two positive CEs at ~255 nm and at ~190 nm, and one negative at ~220 nm in all of the solvents. In the same spectral region in UV spectrum, there is a band at ~193 nm and one shoulder at ~220 nm. One can notice that in the hexane solution the second CE at ~219 nm is blue-shifted by 5 nm in comparison to other solvents, in contrast to the CE at ~197 nm, which is slightly red-shifted by the same value. The magnitude of observed CEs is roughly similar, however in the range of 180-240 nm two bands have a higher intensity in water and lower in hexane. Such a dependency indicates the existence of solvent-solute interaction. On the other hand, a similar shape of UV/ECD curves in four solvents with substantially different polarity points to either the restricted mobility or no-mobility of the cyclohexene ring. In order to investigate the dynamic effects on the equilibrium in solution of (–)-Oseltamivir with a greater detail, and to seek confirmation of earlier conclusion, the low-temperature ECD measurements in a non-polar solvent mixture MI<sub>13</sub> (methylcyclohexane : isopentane, 1:3, *v/v*) at temperatures from +25 °C to -180 °C were done between 210-400 nm (see Fig. S2). As a result, almost no changes in the ECD spectra are observed (Figure S2), indicating a substantial conformational stability.<sup>31</sup> As temperature was lowered, the small decrease of intensity within the lowest energy CE occurs. These changes can be explained by a shift toward the most stable set of conformers. On the other hand, one may claim that ECD spectra of individual conformers do not exhibit features enabling their differentiating in *net* spectrum.

To validate the experimental observations and to elucidate the contributions of possible conformers in the solution phase, the relevant ECD calculations for the first 50 electronic states were performed using 24 structures found during conformational search and subsequent DFT optimization. The simulations of ECD spectra were conducted by TDDFT method and applied the PCM model to reflect solvent influence. The ECD spectra of all conformers were calculated with TZVP, 6-311++G(2d,2p), and aug-cc-pVDZ basis set with two different commonly used functionals for this purpose, *i.e.* B3LYP and CAM-B3LYP. The Boltzmann weighted ECD spectrum reproduced very well the experimental ECD features with all listed combinations of levels of theory. However, CAM-B3LYP/aug-cc-pVDZ with PCM for CH<sub>3</sub>CN gave the best agreement (Fig. 4). The lowest energy band at ~255 nm is

corresponding to the transition, having the character of a double bond and ester  $n(\text{O}) \rightarrow \pi^*$  transitions. The second strong negative band centred at  $\sim 220$  nm is an admixture of transitions linked with  $n(\text{O}) \rightarrow \pi^*$  and  $n(\text{N}) \rightarrow \pi^*$  transitions, while the highest energy band at  $\sim 190$  nm is assigned to the  $\pi \rightarrow \pi^*$  transitions of the ester and amide moiety. An overview of calculated excited-state properties and molecular orbitals involved in the key transitions for **Conf. 5** are placed in the Supporting Information (Table S2 and Fig. S4).

The calculated ECD spectra using PCM model for various solvents are very similar. Therefore, it is clear that there is no discernible solvent effect dependency on ECD curves, independently confirming conclusions from the experimental spectra (Table 3 and Fig. 4).

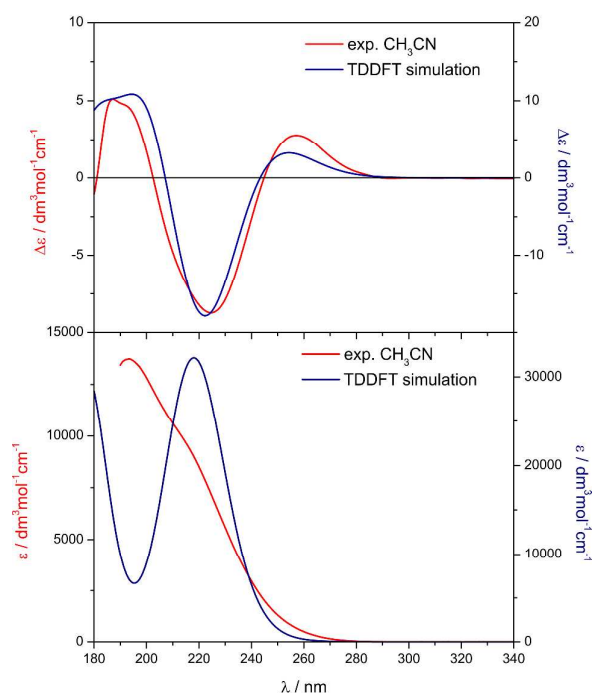


**Fig. 4.** Computed ECD (top) and UV (bottom) spectra using 50 electronic states obtained as a population weighted sum of the calculated spectra of individual conformers of (–)-Oseltamivir compared to experimental spectra recorded in  $\text{CH}_3\text{CN}$ . The UV spectrum simulated using the same bandwidth as ECD (0.4 eV).

To investigate whether more hints about the molecular structure of (–)-Oseltamivir can be derived from ECD spectra, a set of four representative conformers from both families, were selected for more thorough analysis. The first pair of conformers, **Conf. 5** and **Conf. 4**, differing in energy by 0.14 kcal/mol, is most abundant and populated at *ca.* 30% in the equilibrium at 298 K. Both conformers belong to the first family of conformers with a negative C5-C4-N12-C15 torsion angles. The main structural difference between them is related to the orientation of ester substituent, showing both different sign and value of the C2-

C1-C7-O11 torsion angle (Table 2, Fig. 2). As representatives of the second family, less populated in the conformational equilibrium, **Conf. 3** and **Conf. 2** were selected. They both have a positive C5-C4-N12-C15 torsion angle. The difference between them occurs again in the sign of the C2-C1-C7-O11 torsion angle. The predicted ECD spectra show that there are two sets of conformers in the solution, which exhibit the same signs of CEs (directly matching to experimental bands), but with substantially different levels of intensities, especially at ~240 nm and at ~215 nm (Fig. S3). Based on this result, one can anticipate that quantitative analysis of experimental and calculated ECD spectra may give some clues about predominant set of conformers. ECD spectrum recorded in water and acetonitrile shows higher magnitude of CEs, in relation to hexane solution. Consequently, conformers with higher intensity of CEs are favoured in polar solvents, while in non-polar hexane – the dominant set of conformers is that with smaller intensity. Furthermore, a variable temperature ECD spectra (Figure S2) show only a slight decrease of the lowest energy CE intensity, suggesting a stabilisation of conformers with less intense CEs.

#### Analysis of ORD spectra

To find more evidence about conformational equilibrium in a solution of (–)-Oseltamivir, investigation of ORD data was carried out. The experimental ORD spectra were recorded in Vis region (400-700 nm) using three different solvents, *i.e.* CHCl<sub>3</sub>, CH<sub>3</sub>CN, and H<sub>2</sub>O. The results are given in Table 4 and Fig. 5 for six different wavelengths (633, 589, 574, 546, 436, and 405 nm).

**Table 4.** ORD data of (–)-Oseltamivir recorded in chloroform (*c* 0.37), acetonitrile (*c* 0.35), and water (*c* 0.41) at 20 °C.

Solvent	[α] / deg cm <sup>2</sup> g <sup>-1</sup>					
	633 nm	589 nm	574 nm	546 nm	436 nm	405 nm
CHCl <sub>3</sub>	-57	-64	-67	-76	-157	-209
CH <sub>3</sub> CN	-38	-44	-47	-54	-88	-105
H <sub>2</sub> O	-22	-26	-28	-32	-59	-74

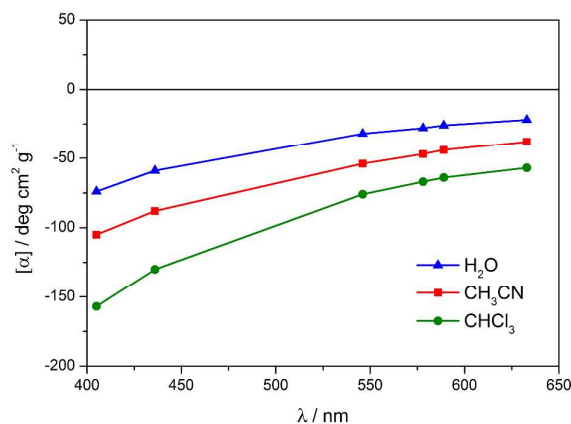


**Fig. 5.** ORD spectra for (–)-Oseltamivir recorded in chloroform, acetonitrile, and water at 20 °C.

These ORD spectra show very similar profiles, but they are of quite different magnitude. The specific rotations depend on the polarity of a solvent. Consequently, in chloroform the magnitude is significantly higher than in water solution. It suggests that the conformation of substituents at C1, C3 and C4 is in some way different, what is reflected in a certain influence on the ORD curves. In order to better understand the experimental results, the TDDFT calculations were performed at the same levels of theory as for ECD, using the identical set of conformers, *i.e.* CAM-B3LYP/aug-cc-pVDZ and B3LYP/aug-cc-pVDZ, with PCM model both for CH<sub>3</sub>CN and CHCl<sub>3</sub>. A comparison between the experimental data and calculated results is reported in Table S3 and Fig. 6.

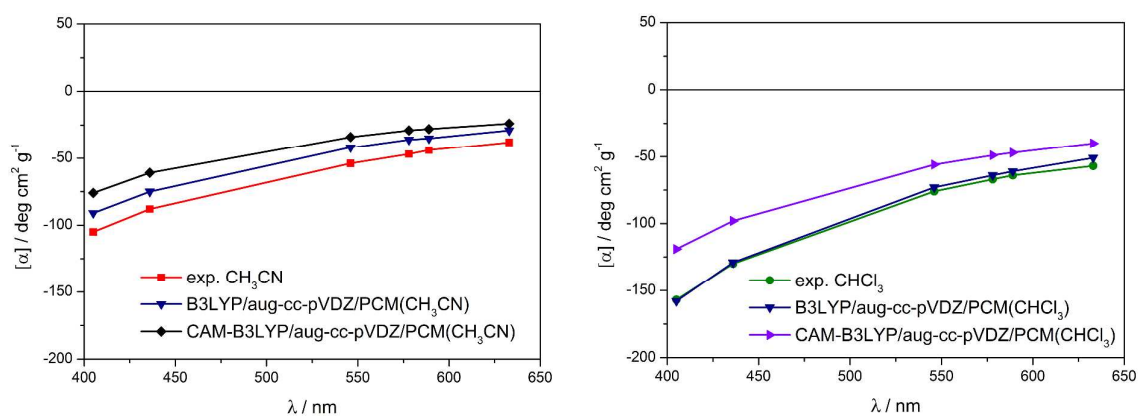


**Fig. 6.** Computed ORD spectra obtained as a population weighted sum of the calculated spectra of individual conformers of (–)-Oseltamivir compared to experimental spectra recorded in CH<sub>3</sub>CN (left) and CHCl<sub>3</sub> (right).

Theoretical ORD spectra show the same sign and trend as the experimental data of (–)-Oseltamivir. In both cases, regardless of the functionals used (B3LYP and CAM-B3LYP), there is a good consistency between the experimental and calculated spectra. An important

point to be noted here is that conformational species in chloroform are different than those in acetonitrile, what can be derived by comparing both experimental and simulated ORD spectra. Moreover, one may conclude that in the chloroform solution, the hydrogen bonds with the solute are not present, in contrast to the acetonitrile solution. Thus, chloroform barely interacts with the solute, having almost negligible effect on the equilibrium in solution. Notwithstanding this and the fact that conformational sensitivity of ORD curves is higher for (–)-Oseltamivir than for ECD, ORD do not reveal the particular details of conformation changes in solution.

### Analysis of VCD spectra

In comparison with ECD, the range of applications of VCD for studying 3D environment of chiral molecules is much greater. A number of possible vibrational transitions lead to a more rigorous definition of molecular structure.<sup>6,11,32-34</sup> Therefore, this method was chosen for the next step of conformational study of (–)-Oseltamivir. Experimental IR and VCD spectra were measured in two solvents, CD<sub>3</sub>CN and CDCl<sub>3</sub> (Fig. 7).

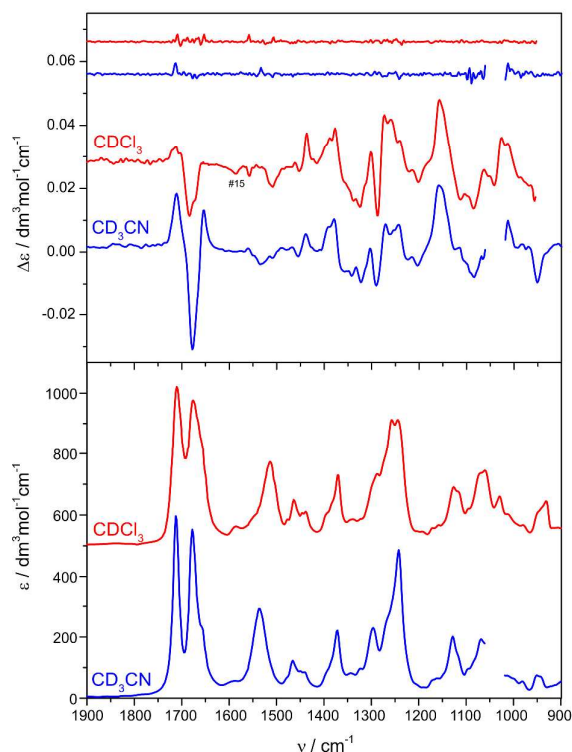


**Fig. 7.** Experimental VCD (top) and IR (bottom) spectra of (–)-Oseltamivir recorded in CD<sub>3</sub>CN and CDCl<sub>3</sub>.

The measurement range can be divided into two sub-regions: (a) the 1900–1600  $\text{cm}^{-1}$ , showing intense absorption bands originating from the C=O stretching vibration from amide and ester groups and C=C bond; (b) the 1600–900  $\text{cm}^{-1}$ , where the so-called *fingerprint* vibrations occur. These transitions represent mainly bending vibrations related to amide, ester and 3-pentyl moieties and cyclohexene ring. The analysis of the main bands by Veda software<sup>35</sup> were summarized in Table S4 in the Supporting Information.

Direct comparison of IR and VCD spectra recorded in two solvents, having significantly different characters, demonstrated no essential differences in the spectral pattern, suggesting that the conformational landscape is similar in the two solvents. However, closer inspection led to the conclusion that some differences can be found in the intensity of the VCD bands in the 1900–1600  $\text{cm}^{-1}$  range, as well as in the 1300–1200  $\text{cm}^{-1}$  range. Furthermore, in IR spectrum the band located at  $\sim 1300 \text{ cm}^{-1}$  in  $\text{CDCl}_3$  occurs as a shoulder, while in  $\text{CD}_3\text{CN}$  it is well resolved. The next band centred at  $\sim 1250 \text{ cm}^{-1}$  in  $\text{CDCl}_3$  splits into two, and exists in  $\text{CD}_3\text{CN}$  as a distinctive feature. In the whole spectrum range a red-shift (from 1 to 21  $\text{cm}^{-1}$ ) of the bands is also observed when going from  $\text{CDCl}_3$  to  $\text{CD}_3\text{CN}$ . It is useful to point out that  $-\text{NH}_2$  bending vibration (labelled as #15) observed as a broad and weak band in IR spectrum at  $\sim 1593 \text{ cm}^{-1}$ , is not observed in the experimental VCD spectrum recorded in  $\text{CD}_3\text{CN}$ , while it can be easily seen in  $\text{CDCl}_3$  (see Fig. 7). Based on the above-mentioned observations, it is clear that the change of solvent induces conformational fluctuations in a solution of (–)-Oseltamivir.

To validate the experimental results the DFT calculations of VCD and IR spectra were run at the same level of approximation, as was done during the geometry optimization, using the identical set of conformers. The PCM model was applied for both  $\text{CH}_3\text{CN}$  and  $\text{CHCl}_3$  solvents. The resulted Boltzmann averaged VCD and IR spectra, weighted on the basis of Gibbs free energies, were almost identical (Fig. S5 in the Supporting Information). Apparently, the PCM model does not reflect the subtle experimental differences between these two solvents. Therefore, only the comparison between the experimental and the calculated data from  $\text{CH}_3\text{CN}$  is taken into consideration (Fig. 8). The Arabic numerals are used to label the corresponding features in the experimental and DFT spectra.

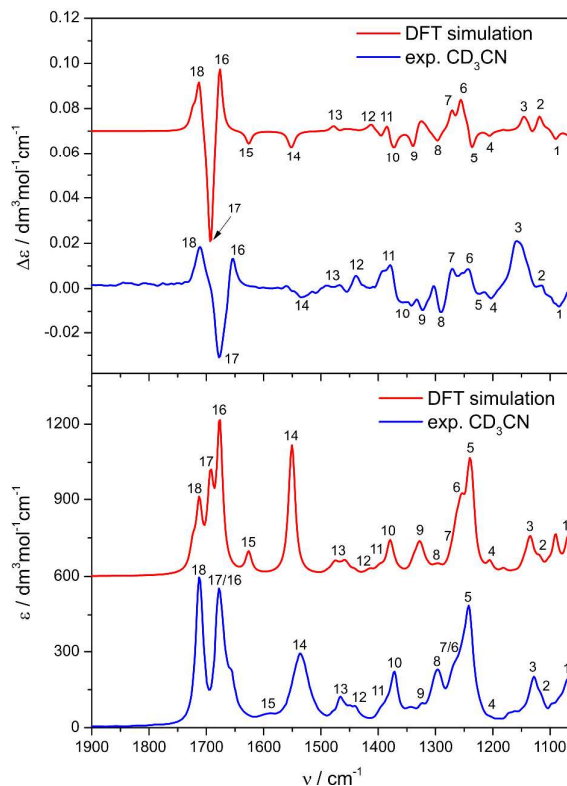


**Fig. 8.** Experimental VCD (top) and IR (bottom) spectra recorded in  $\text{CD}_3\text{CN}$  compared to simulated spectra at the B3LYP/aug-cc-pVDZ/PCM( $\text{CH}_3\text{CN}$ ) level of theory, obtained as a population-weighted sum of the calculated spectra of individual conformers of (-)-Osetamivir. Note that no scaling factor was applied.

As can be seen in Fig. 8, the population-weighted sum spectra are in close agreement with the experimental data. There are only a few features that are not reproduced well by the calculations, and some bands are shifted in comparison with the experimental data. The reason for these discrepancies is most likely related to an underestimation of the dipole and rotatory strengths at the applied level of theory and the fact that the scaling factor was not used over the whole IR and VCD spectrum.

To quantitatively evaluate the agreement between the experimental and theoretical VCD/IR spectra and, in particular, to avoid human bias, a numerical analysis using the CompareVOA<sup>44</sup> software was carried out. The best scaling factor in the measurement range amounts to 0.990, giving the similarity index for IR=86.3% and for VCD=66%. The enantiomer similarity index, calculated as a difference between the similarities for the correct enantiomer (in this case 70%) and the opposite enantiomer (12%) was equal to 58%.

To further increase the reliability of the calculated VCD bands, the robustness analysis, introduced originally by Nicu et al.,<sup>36,37</sup> was performed. The robustness analysis of

(-)-Oseltamivir carried out on **Conf. 5**, showed that all VCD bands, except for one at 1535  $\text{cm}^{-1}$  (#14), have a  $\zeta$  ratio higher than 10 ppm (Table S4). Consequently, these bands are robust and can therefore bring reliable structural information. Furthermore,  $g$ -factor for band #14 equals  $1 \times 10^{-5}$  and from experimental point of view VCD signal may be highly permuted by noise and experimental parameters.<sup>38</sup>

When considering molecules with group(s) which can form intermolecular H-bond(s) with the solvent (in this case  $\text{CH}_3\text{CONH-}$  and  $-\text{NH}_2$  groups with  $\text{CH}_3\text{CN}$ ) one may expect some additional interactions that could affect the conformational equilibrium. Nevertheless, the correct shape of VCD and IR spectra was captured quite accurately, so further discussion of problems with application of explicit solvent model approach extends beyond the framework of this study. On the other hand, vibrational spectra of (-)-Oseltamivir do not provide definitive proof for the set of the predominate conformers in these two solvents. It should not be surprising since the most abundant conformers in chloroform and acetonitrile, *i.e.* **Conf. 1** and **Conf. 5** respectively, are very similar and differ only in orientation of ethyl group in ester moiety (Fig. 2 and Table 2), and therefore their VCD spectra are very similar (Fig. S6). Additionally, such a flexible molecule possess no conformation(s) with apparently leading weight, what is manifested in experimental vibrational optical activity data.

### Analysis of ROA spectra

Raman optical activity (ROA) is currently recognized as an excellent tool for structural studies of various bioorganic systems.<sup>39-42</sup> The advantage of applying ROA in structural studies, instead of VCD, stems from the fact that ROA enables a direct examination of biomolecules in their natural/aqueous environment over a broad spectral range, thereby offering a rich information content.

With this background in mind, the Raman and ROA spectra were measured in aqueous solution with excitation at 532 nm in the range of 2000-100  $\text{cm}^{-1}$ . The comparison of experimental data with the simulated spectra of the most abundant conformers found during the conformational analysis at B3LYP/aug-cc-pVDZ/PCM( $\text{H}_2\text{O}$ ) level is presented in Fig. 9. Based on the available literature reports, many authors<sup>43,44</sup> have valued this level of approximation as being fairly effective, although PCM model is far from being a perfect tool for the simulation of the influence of an aqueous environment on solute.<sup>45</sup> The most intense bands in Raman spectrum were found in the region of 1800-1600  $\text{cm}^{-1}$  and they are related to the C=O stretching vibrations of amide and ester groups, overlapped with vibration from the

C=C bond. In contrast, the ROA spectrum in this region is not characteristic and informative, and only three very weak bands can be observed. The most intense ROA region ( $1500\text{--}1250\text{ cm}^{-1}$ ) is associated mostly with the bending vibrations of amide, ester groups and cyclohexene ring.

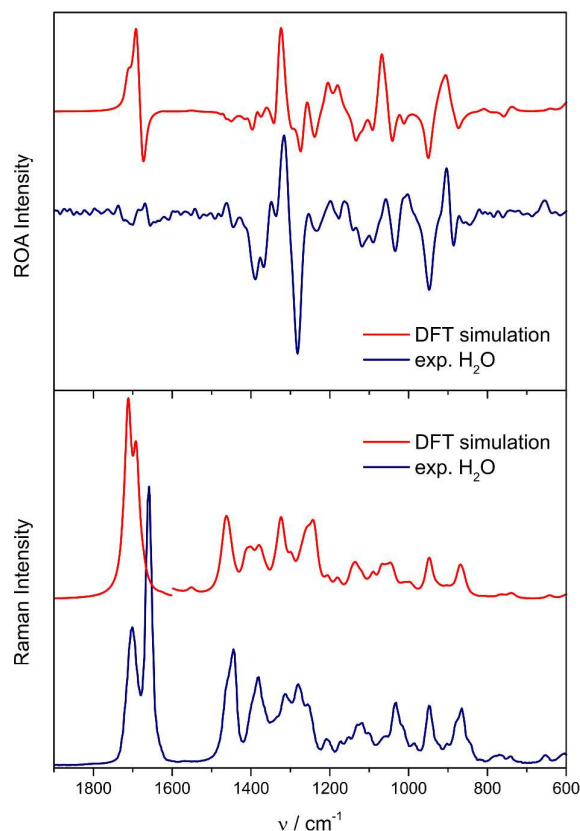


**Fig. 9.** Experimental ROA (top) and Raman (bottom) spectra recorded in  $\text{H}_2\text{O}$  compared to simulated spectra at the B3LYP/aug-cc-pVDZ/PCM( $\text{H}_2\text{O}$ ) level of theory, obtained as a population-weighted sum of the calculated spectra of individual conformers of (–)-Oseltamivir. Note that no scaling factor was applied. The range  $1600\text{--}600\text{ cm}^{-1}$  multiplies by 3.

In the Boltzmann-averaged spectra the highest inconsistency is present only in ROA spectrum in the range of  $1800\text{--}1600\text{ cm}^{-1}$ , in contrast to the Raman spectrum, where all features are well reproduced. Generally, ROA calculations are notoriously difficult from the purely theoretical and the computational point of view.<sup>39,40</sup> However, this observation indicates that H-bonds formation between (–)-Oseltamivir and solvent molecules exist, what is not so clearly visible while using other chiroptical spectra.

The above discussion leads to the conclusion that the DFT calculations of chiroptical spectra confirm the strength of the conformational analysis performed for water as a solvent

and provide further support for conclusion derived from VCD spectroscopy, namely that the chosen set of the most abundant conformers in solution of acetonitrile and water is convergent. However, due to the high flexibility of (–)-Oseltamivir and the presence of groups responsible for hydrogen bonding, a definitive answer cannot be given. In addition, ROA spectrum, among previously used chiroptical methods, provided additional insight into solute-solvent interactions (in the range of 1800-1600  $\text{cm}^{-1}$ ). It suggests that conformer distribution in water solution is disturbed by intermolecular interactions, so the presence of **Conf. 5** as the major component of population cannot be unambiguously proved.

### X-Ray structure vs. DFT calculated structures

The solid-state molecular structure derived from the single crystal X-ray diffraction analysis of (–)-Oseltamivir Phosphate, recently published by Naumov (CCDC 914529),<sup>18,19</sup> was compared to the most stable conformation (**Conf. 5**) in water solution calculated at the B3LYP/aug-cc-pVTZ/PCM(H<sub>2</sub>O) level of theory. (–)-Oseltamivir Phosphate crystallizes without solvent in the chiral  $P2_12_12$  space group, and the asymmetric unit contains two independent ion pairs slightly differing in geometry, therefore Fig. 10 and Table S5 show the comparison between these two molecules, namely A and B, and **Conf. 5**.

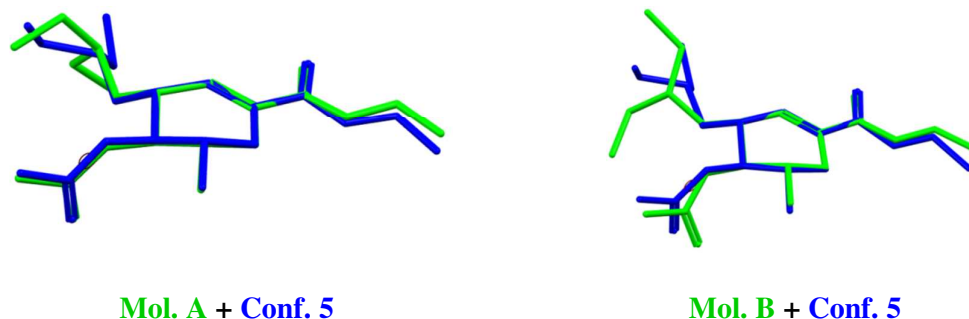


**Fig. 10.** Comparison of the X-ray structure of (–)-Oseltamivir Phosphate<sup>19</sup> (green) with the structure of the lowest energy conformer **Conf. 5** (blue) of (–)-Oseltamivir in water calculated at the B3LYP/aug-cc-pVDZ(H<sub>2</sub>O) level of theory. **Left:** overlay of crystallographic structure of molecule A and the computed structure; **Right:** overlay of crystallographic structure of molecule B and the computed structure. Hydrogen atoms as well as phosphate group (H<sub>2</sub>PO<sub>4</sub><sup>−</sup>) were dismissed for clarity.

Amongst all 24 structures found during conformational analysis, **Conf. 5** which is that of the lowest energy conformation of (–)-Oseltamivir determined by molecular modeling performed in acetonitrile and water, is the most similar to the structure obtained from the X-ray data. Since molecules in the solid-state are linked by the intermolecular interaction, it is

natural that some small inevitable differences occur due to both the conformational and vicinal effects. The only noticeable difference is related to the orientation of 3-pentyl group at C3 position. However, this part of molecule has the highest mobility and it is expected that in a solution a number of rotamers will be present. It is worth to emphasize that the differences in torsion angles of cyclohexene ring are very small in comparison to DFT calculations, due to the high rigidity of (–)-Oseltamivir skeleton.

## CONCLUSIONS

To get deeper insight into the solution stereochemistry of (–)-Oseltamivir, the simultaneous application of various chiroptical methods, *i.e.* ECD, ORD, VCD, ROA, assisted by computational calculations has been described in this work. It appears that this is the first case of such a comprehensive study. Based on the extensive conformational search, the relevant conformational landscape of (–)-Oseltamivir was determined. Close similarity of geometry of the lowest energy Conf. 5 and recently published X-ray structure of (–)-Oseltamivir Phosphate<sup>18,19</sup> leads to conclusion that this conformation may predominate also in the solution of (–)-Oseltamivir. However, a relatively large number of similar structures detected in chloroform, acetonitrile and water solutions pose a challenge for selecting the dominant structure uniquely.

Taking advantage of multi-chiroptical approach utilized within the work the following findings were noted:

- temperature and solvent-dependent ECD curves indicate the conformational dynamics combined with electronic structure;
- ORD spectra measured in chloroform, acetonitrile and water show considerable solvent impact on the conformational equilibrium;
- VCD data further reveal conformational changes and influence of the environment on solution equilibrium. They are particularly present in the range of 1800-1600cm<sup>-1</sup>, where C=O stretching vibration of amide and ester groups as well as C=C bond appear;
- ROA spectrum shows that solute-solvent interactions resulting mainly from hydrogen bonding, play a significant role in the water solution of (–)-Oseltamivir.

Considering the above results, it can be concluded that diverse conformers are stable in chloroform, acetonitrile and water solution. The solvent influence is particularly noticeable for an aqueous environment. In the light of these results, one may state that knowledge about

the single crystal X-ray structure of such a flexible molecule may not be sufficient enough to thoroughly identify the enzyme-bound conformations inhibiting the influenza.

Additionally, the data presented in the present work clearly demonstrate that the simultaneous application of chiroptical techniques provides more complete structure inspection of APIs in solutions.

## EXPERIMENTAL SECTION

**ECD Measurements.** The experimental ECD spectra were recorded using Jasco J-815 spectrometer at room temperature in spectroscopic grade hexane,  $\text{CHCl}_3$ ,  $\text{CH}_3\text{CN}$ , and water. Solutions with concentration of  $\sim 5 \times 10^{-4}$  M were measured in a quartz cell with a path length of 1–0.1 cm. All spectra were recorded using a scanning speed of 100 nm/min, a step size of 0.2 nm, a bandwidth of 1 nm, a response time of 0.5 s, and an accumulation of 5 scans. The spectra were background-corrected using spectra of respective solvents recorded under the same conditions.

**ORD Measurements.** The experimental ORD spectra were recorded using Jasco J-815 spectropolarimeter equipped with Optical Rotatory Dispersion mode attachment (ORD-M401) at 20 °C temperature in spectroscopic grade  $\text{CHCl}_3$ ,  $\text{CH}_3\text{CN}$ , and  $\text{H}_2\text{O}$  in the range of 400–700 nm. Solutions with concentration  $\sim 1 \times 10^{-2}$  M were measured in a quartz cell with a 1 cm path length placed in Peltier type cell holder. All spectra were recorded using a scanning speed of 100 nm/min, a step size of 0.5 nm, a bandwidth of 4 nm, a response time of 4 s, and an accumulation of 3 scans. The spectra were background-corrected using spectra of respective solvents recorded under the same conditions.

**VCD Measurements.** The VCD and IR spectra were collected simultaneously using ChiralIR-2X FT-VCD spectrometer from BioTools Inc. at a resolution of  $4 \text{ cm}^{-1}$  in the range of 2000–850  $\text{cm}^{-1}$  using  $\text{CD}_3\text{CN}$  and  $\text{CHCl}_3$ . The spectrometer was equipped with dual sources and dual ZnSe photoelastic modulators (PEMs) optimized at 1400  $\text{cm}^{-1}$ . A solution with a concentration of 0.16 M was measured in a  $\text{BaF}_2$  cell with a path length of 102  $\mu\text{m}$  assembled in a rotating holder. To improve the signal-to-noise ratio, the spectra were measured for 6 h. Baseline correction was achieved by subtracting the spectrum of a solvent recorded under the same conditions.

**ROA Measurements.** The ROA and Raman spectra were collected simultaneously using ChiralRaman-2X spectrometer from BioTools Inc. at a resolution of  $\sim 7 \text{ cm}^{-1}$  in the range of

2000–100  $\text{cm}^{-1}$  using an excitation wavelength of 532 nm. An aqueous solution with a concentration of 0.49 M was measured in a micro fluorescence quartz cell with a path length of 3 mm. The laser power was set to 600 mW at the source. Spectral acquisition times were ~17 h (59040 scans). The baseline was corrected by subtracting the spectrum obtained for the solvent recorded under the same conditions.

## COMPUTATIONAL METHODS

**Conformational Analysis.** The initial conformational search was done using CONFLEX 7<sup>21-</sup><sup>23</sup> software with the MMFF94s force fields within 10 kcal/mol energy window. Next, all obtained structures were submitted to the Gaussian09<sup>24</sup> program for DFT optimisation. First, the B3LYP/6-31G(d) level of theory was used to reduce the total number of found conformers, eliminating those that do not have a strong impact on the overall population. Then the remaining conformers were re-optimized using a set of different levels of theory, *i.e.*, B3LYP/TZVP, B3LYP/6-311++G(2d,2p), B3LYP/aug-cc-pVDZ, and CAM-B3LYP/aug-cc-pVDZ, with the implicit polarizable continuum model (PCM)<sup>26</sup> for  $\text{CHCl}_3$ ,  $\text{CH}_3\text{CN}$ , and  $\text{H}_2\text{O}$ . All conformers were confirmed to contain no imaginary frequencies, so they represent the real minima. The obtained results were similar for all the applied theory levels. Therefore, the final 24 structures with geometry obtained at B3LYP/aug-cc-pVDZ/PCM were chosen for subsequent simulations of ECD, ORD, VCD and ROA spectra. Boltzmann populations were derived from the relative Gibbs energies ( $\Delta G$ ) of individual conformers calculated at 298 K.

**ECD Simulations.** Theoretical ECD and UV spectra were computed at the TDDFT CAM-B3LYP/aug-cc-pVDZ level using PCM model for  $\text{CH}_3\text{CN}$  based on the geometry taken from the B3LYP/aug-cc-pVDZ/PCM( $\text{CH}_3\text{CN}$ ) level. Furthermore, the ECD spectra were calculated using TZVP and 6-311++G(2d,2p) basis set with B3LYP and CAM-B3LYP. Calculations were performed for the first 50 excited electronic states, which cover the spectral range of 150-300 nm. However, it has been noticed that the 15 electronic transitions span the range of 170-300 nm. Rotatory strengths were calculated using both the length and the velocity formalisms. The differences between these two were less than 5%, and for this reason, only the velocity representations ( $R_{\text{vel}}$ ) were taken into account. The final spectrum was obtained by Boltzmann averaging ( $T = 298 \text{ K}$ ), according to the population percentages of the individual conformers. The ECD spectra were simulated by overlapping Gaussian functions for each transition (0.4 eV bandwidth) using the SpecDis<sup>46,47</sup> software.

**ORD Simulations.** Optical rotations were calculated at six wavelengths (633, 589, 574, 546, 436, and 405 nm) using the TDDFT CAM-B3LYP and B3LYP functional, as well as aug-cc-pVDZ basis set with PCM model for CH<sub>3</sub>CN and CHCl<sub>3</sub>. The final spectrum was obtained by Boltzmann averaging ( $T = 298$  K), according to the population percentages of the individual conformers.

**VCD Simulations.** Theoretical VCD and IR spectra were calculated at the B3LYP/aug-cc-pVDZ level with PCM model for CH<sub>3</sub>CN and CHCl<sub>3</sub>. The final spectrum was obtained by Boltzmann averaging ( $T = 298$  K), according to the population percentages of the individual conformers. The Boltzmann-averaged spectrum, was converted to Lorentzian bands with a 6 cm<sup>-1</sup> half-width at half-peak height. The frequencies were not scaled.

**ROA Simulations.** Theoretical ROA and Raman spectra were calculated at the B3LYP/aug-cc-pVDZ level with PCM model for H<sub>2</sub>O. The final spectrum was obtained by Boltzmann averaging ( $T = 298$  K), according to the population percentages of the individual conformers. The Boltzmann-averaged spectrum, was converted to Lorentzian bands with a 10 cm<sup>-1</sup> half-width at half-peak height. The frequencies were not scaled.

## ASSOCIATED CONTENT

A complete overview of the conformational search for the (-)-Oseltamivir. Low-temperature ECD measurements. Comparison of computed ECD and VCD spectra of selected representative conformers. Vibrational analysis for the Conf. 5. Cartesian coordinates of all calculated conformers.

## ACKNOWLEDGEMENTS

This work was funded by Grant No. UMO-2011/03/N/ST4/02426 from the National Science Centre (Poland). All computational calculations were performed at the Interdisciplinary Centre for Mathematical and Computational Modeling (ICM) of University of Warsaw (grant No. G34-15). The author acknowledges Prof. Jadwiga Frelek for helpful and inspiring discussions, Prof. Wojciech J. Szczypek for providing sample of (-)-Oseltamivir, and Dr. Elemér Vass for his very kind help with the ROA measurements.

## REFERENCES

1. R. Sardella, A. Carotti, G. Manfroni, D. Tedesco, A. Martelli, C. Bertucci, V. Cecchetti and B. Natalini, *J. Chrom. A*, 2014, **1363**, 162–168.

2. D. Tedesco, R. Zanasi, I. W. Wainer and C. Bertucci, *J. Pharm. Biomed. Anal.*, 2014, **91**, 92-96.
3. W. H. Brooks, W. C. Guida and K. G. Daniel, *Curr. Top. Med. Chem.*, 2011, **11**, 760-770.
4. M. Górecki, A. Suszczyńska, M. Woźnica, A. Baj, M. Wolniak, M. K. Cyrański, S. Witkowski and J. Frelek, *Org. Biomol. Chem.*, 2014, **12**, 2235-2254.
5. K. Knapp, M. Górecki, J. Frelek, R. Luboradzki, M. Hollósi, Z. Majer and E. Vass, *Chirality*, 2014, **26**, 228-242.
6. X. Li, K. H. Hopmann, J. Hudecová, J. Isaksson, J. Novotná, W. Stensen, V. Andrushchenko, M. Urbanová, J.-S. Svendsen, P. Bouř and K. Ruud, *J. Phys. Chem. A*, 2013, **117**, 1721-1736.
7. G. SzilvÁgyi, Z. Majer, E. Vass and M. Hollósi, *Chirality*, 2011, **23**, 294-299.
8. V. P. Nicu, A. Mándi, T. Kurtán and P. L. Polavarapu, *Chirality*, 2014, **26**, 525-531.
9. S. Abbate, G. Longhi, F. Lebon, E. Castiglioni, S. Superchi, L. Pisani, F. Fontana, F. Torricelli, T. Caronna, C. Villani, R. Sabia, M. Tommasini, A. Lucotti, D. Mendola, A. Mele and D. A. Lightner, *J. Phys. Chem. C*, 2013, **118**, 1682-1695.
10. P. Scafato, F. Caprioli, L. Pisani, D. Padula, F. Santoro, G. Mazzeo, S. Abbate, F. Lebon and G. Longhi, *Tetrahedron*, 2013, **69**, 10752-10762.
11. J. Sadlej, J. C. Dobrowolski and J. E. Rode, *Chem. Soc. Rev.*, 2010, **39**, 1478-1488.
12. J. E. Rode, J. C. Dobrowolski and J. Sadlej, *J. Phys. Chem. B*, 2013, **117**, 14202-14214.
13. P. L. Polavarapu, *Chirality*, 2008, **20**, 664-672.
14. A. G. Petrovic, A. Navarro-Vázquez and J. L. Alonso-Gómez, *Curr. Org. Chem.*, 2010, **14**, 1612-1628.
15. E. J. Corey, B. Czako and L. Kurti, *Molecules and Medicine*, Wiley, Hoboken, 2007.
16. M. Karchier, K. Michalak and J. Wicha, *Wiad. Chem.*, 2007, **61**, 7-42.
17. T. Mukaiyama, H. Ishikawa, H. Koshino and Y. Hayashi *Chem. Eur. J.*, 2013, **19**, 17789-17800.
18. P. Naumov, N. Yasuda, W. M. Rabeh and J. Bernstein, *Chem. Commun.*, 2013, **49**, 1948-1950.
19. Cambridge Crystallographic Data Centre, No CCDC 914529.
20. A. Mazzanti and D. Casarini, *WIREs: Computational Molecular Science*, 2012, **2**, 613-641.
21. *CONFLEX 7*, Conflex Corp., Japan, 2012.
22. H. Goto and E. Osawa, *J. Am. Chem. Soc.*, 1989, **111**, 8950-8951.
23. H. Goto and E. Osawa, *J. Chem. Soc., Perkin Trans. 2*, 1993, 187-198.
24. M. J. Frisch, G. W. Trucks, H. B. Schlegel, G. E. Scuseria, M. A. Robb, J. R. Cheeseman, G. Scalmani, V. Barone, B. Mennucci, G. A. Petersson, H. Nakatsuji, M. Caricato, X. Li, H. P. Hratchian, A. F. Izmaylov, J. Bloino, G. Zheng, J. L. Sonnenberg, M. Hada, M. Ehara, K. Toyota, R. Fukuda, J. Hasegawa, M. Ishida, T. Nakajima, Y. Honda, O. Kitao, H. Nakai, T. Vreven, J. A. Montgomery Jr., J. E. Peralta, F. Ogliaro, M. J. Bearpark, J. Heyd, E. N. Brothers, K. N. Kudin, V. N. Staroverov, R. Kobayashi, J. Normand, K. Raghavachari, A. P. Rendell, J. C. Burant, S. S. Iyengar, J. Tomasi, M. Cossi, N. Rega, N. J. Millam, M. Klene, J. E. Knox, J. B.

- Cross, V. Bakken, C. Adamo, J. Jaramillo, R. Gomperts, R. E. Stratmann, O. Yazyev, A. J. Austin, R. Cammi, C. Pomelli, J. W. Ochterski, R. L. Martin, K. Morokuma, V. G. Zakrzewski, G. A. Voth, P. Salvador, J. J. Dannenberg, S. Dapprich, A. D. Daniels, Ö. Farkas, J. B. Foresman, J. V. Ortiz, J. Cioslowski and D. J. Fox, *Gaussian 09*, Revision D.01, Gaussian, Inc., Wallingford, CT, 2013.
25. L. Di Bari and G. Pescitelli, *Electronic Circular Dichroism*, in *Computational Spectroscopy: Methods, Experiments and Applications* edn., Wiley, Weinheim, 2010.
  26. M. Cossi, G. Scalmani, N. Rega and V. Barone, *J. Chem. Phys.*, 2002, **117**, 43-54.
  27. C. Reichardt, *Solvents and Solvent Effects in Organic Chemistry*, Wiley, Weinheim, 2010.
  28. M. Pecul, *Modeling of solvation effects on chiroptical spectra*, in *Comprehensive Chiroptical Spectroscopy* edn., Vol. 1, Wiley, New York, 2012.
  29. P. L. Polavarapu, G. Scalmani, E. K. Hawkins, C. Rizzo, N. Jeirath, I. Ibnu Saud, D. Habel, D. S. Nair and S. Haleema, *J. Nat. Prod.*, 2011, **74**, 321-328.
  30. F. Weber and R. Brückner, *Chem. Eur. J.*, 2013, **19**, 1288-1302.
  31. A. Moscowitz, K. M. Wellman and C. Djerassi, *J. Am. Chem. Soc.*, 1963, **85**, 3515-3516.
  32. P. L. Polavarapu, J. Frelek and M. Woźnica, *Tetrahedron: Asymmetry* 2011, **22**, 1720-1724.
  33. M. Górecki, A. Karczmarzka-Wódzka, R. Kołodziejaska, M. Dramiński and J. Frelek, *Eur. J. Org. Chem.*, 2014, **24**, 5204-5213.
  34. E. D. Gussem, P. Bultinck, M. Feledziak, J. Marchand-Brynaert, C. V. Stevens and W. Herrebout, *Phys. Chem. Chem. Phys.*, 2012, **14**, 8562-8571.
  35. M. H. Jamróz, *Vibrational Energy Distribution Analysis VEDA 4 software*, Warsaw, 2010.
  36. V. P. Nicu, J. Neugebauer and E. J. Baerends, *J. Phys. Chem. A*, 2008, **112**, 6978-6991.
  37. S. Gobi and G. Magyarfalvi, *Phys. Chem. Chem. Phys.*, 2011, **13**, 16130-16133.
  38. C. L. Covington and P. L. Polavarapu, *J. Phys. Chem. A*, 2013, **117**, 3377-3386.
  39. M. Barańska (Ed.), *Optical Spectroscopy and Computational Methods in Biology and Medicine*, Springer, 2014.
  40. L. A. Nafie, *Vibrational Optical Activity: Principles and Applications*, Wiley, 2011.
  41. L. D. Barron and A. D. Buckingham, *Chem. Phys. Lett.*, 2010, **492**, 199-213.
  42. V. Parchansky, J. Kapitan and P. Bour, *RSC Adv.*, 2014, **4**, 57125-57136.
  43. J. C. Dobrowolski, M. H. Jamróz, R. Kolos, J. E. Rode, M. K. Cyrański and J. Sadlej, *Phys. Chem. Chem. Phys.*, 2010, **12**, 10818-10830.
  44. M. Kamiński, A. Kudelski and M. Pecul, *J. Phys. Chem. B*, 2012, **116**, 4976-4990.
  45. K. H. Hopmann, K. Ruud, M. Pecul, A. Kudelski, M. Dračinský and P. Bour, *J. Phys. Chem. B*, 2011, **115**, 4128-4137.
  46. T. Bruhn, Y. Hemberger, A. Schaumlöffel and G. Bringmann, *SpecDis 1.62*, University of Würzburg, Germany, 2013.
  47. T. Bruhn, A. Schaumlöffel, Y. Hemberger and G. Bringmann, *Chirality*, 2013, **25**, 243-249.

